Evolution and mechanism from structures of an ADP-ribosylating toxin and NAD complex

Seungil Han[1], Joyce A. Craig[2], Christopher D. Putnam[1], Nadine B. Carozzi[2] and John A. Tainer[1]

[1]*Department of Molecular Biology and the Skaggs Institute for Chemical Biology, The Scripps Research Institute, La Jolla, California, 92037, USA.* [2]*Novartis Agribusiness Biotechnology Research, Inc., P.O. Box 12257, 3054 Cornwallis Road, Research Triangle Park, North Carolina, 27709-2257, USA.*

A member of the *Bacillus*-produced vegetative insecticidal proteins (VIPs) possesses high specificity against the major insect pest, corn rootworms, and belongs to a class of binary toxins and regulators of biological pathways distinct from classical A-B toxins. The 1.5 Å resolution crystal structure of the enzymatic ADP-ribosyltransferase component, VIP2, from *Bacillus cereus* reveals structurally homologous N- and C-terminal α/β domains likely representing the entire class of binary toxins and implying evolutionary relationships between families of ADP-ribosylating toxins. The crystal structure of the kinetically trapped VIP2–NAD complex identifies the NAD binding cleft within the C-terminal enzymatic domain and provides a structural basis for understanding the targeting and catalysis of the medically and environmentally important binary toxins. These structures furthermore provide specific experimental results to help resolve paradoxes regarding the specific mechanism of ADP-ribosylation of actin by implicating ground state destabilization and nicotinamide product sequestration as the major driving forces for catalysis.

ADP-ribosylating enzymes have key biological functions in defensive cytotoxicity, pathogenicity, intracellular signaling, DNA repair and cell division. These enzymes catalyze the transfer of the ADP-ribose group of NAD to a target protein with nicotinamide release. A novel family of insecticidal ADP-ribosyltransferases were isolated from *Bacillus cereus* during vegetative growth, where VIP1 likely targets insect cells and VIP2 ribosylates actin[1]. Although the extensively used and completely distinct *Bacillus thuringiensis* δ-endotoxins show no activity against western corn rootworm (WCR) and northern corn rootworm (NCR)[1], the VIP1-VIP2 binary toxin is an effective pesticide at 20–40 ng per g diet against these pests. WCR is a serious problem for maize[2].

The VIP1-VIP2 toxin is representative of a class of binary toxins distinct from the classical A-B toxins, such as cholera toxin, that must assemble into a complex composed of two functionally different subunits or domains for activity[3]. Each polypeptide in the VIP1-VIP2 class of binary toxins evidently functions separately, with the membrane-binding 100 kDa VIP1 multimer ostensively providing a pathway for the 52 kDa VIP2 ADP-ribosylase to enter the cytoplasm of target WCR cells[4]. Both VIP1 and VIP2 are required for maximal activity against WCR[1]. The NAD-dependent ADP-ribosyltransferase VIP2 likely modifies monomeric actin at Arg 177 to block polymerization, leading to loss of the actin cytoskeleton and eventual cell death due to the rapid subunit exchange within actin filaments *in vivo*[5]. As VIP2 shares significant sequence similarity with enzymatic components of other binary toxins, *Clostridium botulinum* C2 toxin[6], *C. perfringens* iota toxin[7], *C. piroforme* toxin[8] and *C. difficile* toxin[9], VIP2 represents a family of actin-ADP-ribosylating toxins. However, no crystal structures of this distinct class of binary toxins have been reported. Thus, the structures of VIP2 reported here provide a framework for understanding the mode of action and the mechanism of ADP ribosylation for binary toxins.

Overall structure

The enzyme structures of *B. cereus* VIP2 at 1.5 Å resolution and the complex of VIP2 with NAD at 2.7 Å resolution were determined by multiple isomorphous replacement methods (Table 1). The enzyme structure spans residues 60–461 for four crystallographically independent VIP2 proteins in the uncomplexed structure. VIP2 is a mixed α/β protein (Fig. 1*a–c*) and is divided into two domains, herein termed the N-domain (residues 60–265) and the C-domain (residues 266–461). The domains are structurally homologous despite limited sequence identity (22%) (Fig. 2). Each domain core is formed mainly by perpendicular packing of a five-stranded mixed β-sheet against a three-stranded antiparallel β-sheet. The three-stranded sheet is flanked by four consecutive α-helices and the five-stranded sheet by an additional α-helix. The overall fold of each domain resembles the catalytic domains of classical A-B toxins[10–12], despite the poor sequence similarity both with the catalytic domains of these toxins and between the individual VIP2 domains.

A central cleft, which is formed between the four consecutive α-helices and the five-stranded β-sheet and lined by α8 and four β-strands (β9, β10, β11, and β14), forms the NAD binding pocket in the C-domain. Notably, the four crystallographically independent molecules in the unbound structure have two distinct conformations corresponding to open and closed states, which are related by a hinge motion with a rotation of approximately 6° on an axis formed by a line connecting Cα atoms of residues 276 and 376 (Fig. 1*c*). Least-squares superposition indicates that this hinge motion primarily moves the four consecutive α-helices relative to the rest of the protein. For both of these unbound conformations, the NAD-binding pocket is preformed (Fig. 1*d*). In contrast, the VIP2-NAD complex possesses a single conformational state of the hinge corresponding to a 3° rotation, midway between the open and closed conformation. Thus, NAD binding promotes an intermediate conformation that partially sequesters NAD from solvent, while remaining sufficiently open for direct binding and ADP ribosylation of actin.

Domain structure and evolution

VIP2 domain packing involves distinct surfaces on both domains to generate a nonsymmetrical two-domain structure with implications for functional asymmetry and evolution of the full-length protein. The N- and C-domains are oriented roughly perpendicular to each other, but their central clefts point toward the same face of the molecule. This orientation places two strands of the C-domain (β15 and β16) to block the N-domain cleft while allowing the C-domain NAD-binding cleft to be unhindered. The C-domain of VIP2 is homologous to a class of single-domain Rho-ADP-ribosylating toxins of unknown structures represented by the C3 exoenzyme from *C. botulinum*[13], with which it shares >30% sequence identity, including residues needed for the protein fold and catalysis. This homology and our structural results suggest that the

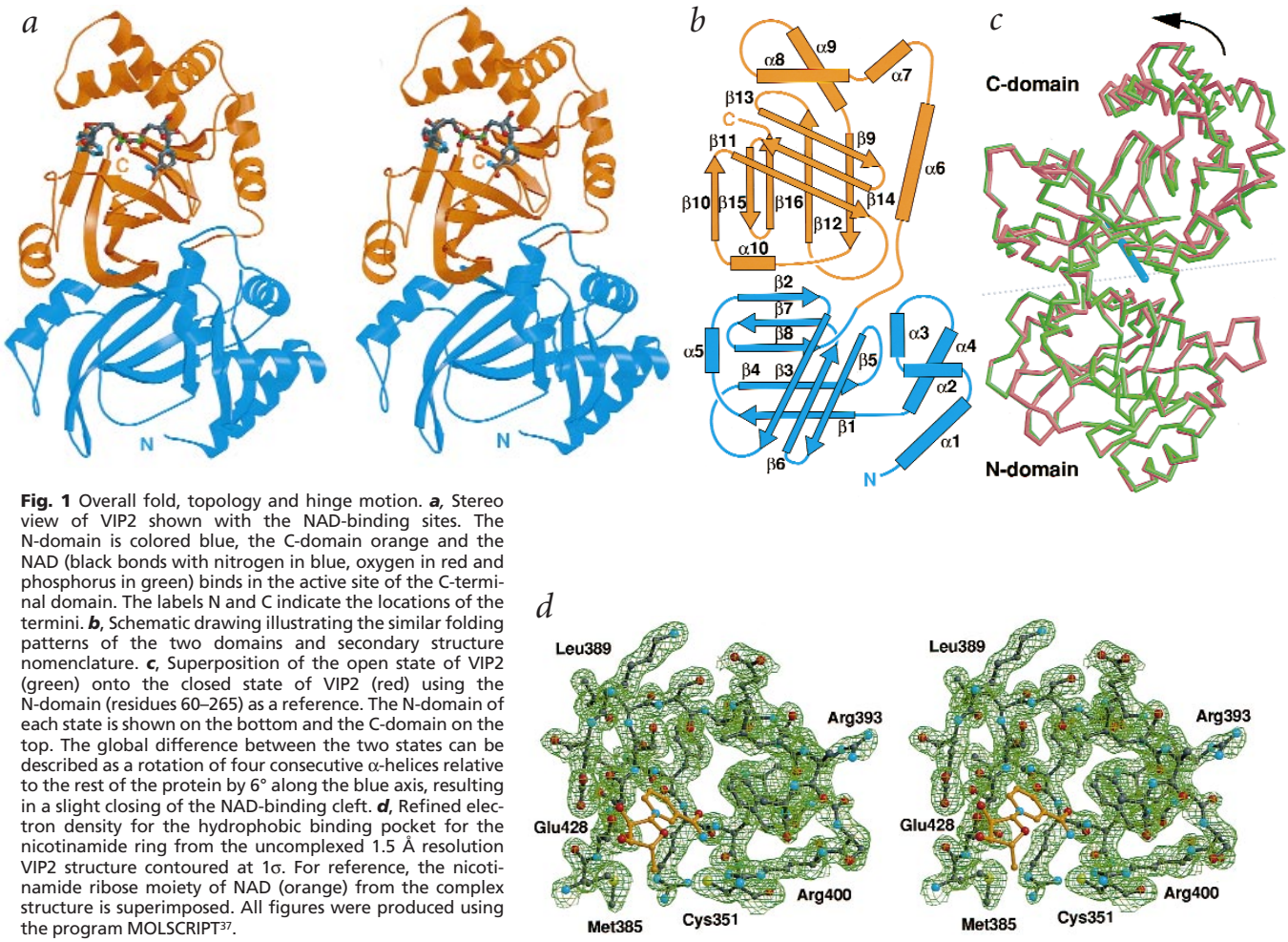

Fig. 1 Overall fold, topology and hinge motion. ***a***, Stereo view of VIP2 shown with the NAD-binding sites. The N-domain is colored blue, the C-domain orange and the NAD (black bonds with nitrogen in blue, oxygen in red and phosphorus in green) binds in the active site of the C-terminal domain. The labels N and C indicate the locations of the termini. ***b***, Schematic drawing illustrating the similar folding patterns of the two domains and secondary structure nomenclature. ***c***, Superposition of the open state of VIP2 (green) onto the closed state of VIP2 (red) using the N-domain (residues 60–265) as a reference. The N-domain of each state is shown on the bottom and the C-domain on the top. The global difference between the two states can be described as a rotation of four consecutive α-helices relative to the rest of the protein by 6° along the blue axis, resulting in a slight closing of the NAD-binding cleft. ***d***, Refined electron density for the hydrophobic binding pocket for the nicotinamide ring from the uncomplexed 1.5 Å resolution VIP2 structure contoured at 1σ. For reference, the nicotinamide ribose moiety of NAD (orange) from the complex structure is superimposed. All figures were produced using the program MOLSCRIPT[37].

VIP2 class of binary toxins has arisen by gene duplication of an ancestral ADP-ribosyltransferase. Importantly, by blocking the central cleft of the N-domain, this gene duplication has impeded the N-domain catalytic function leaving it free to diverge for other functions. Unlike the catalytic C-domain, the extant N-domain is rigid and has been shown by fusion protein studies with the enzymatic components of *C. botulinum* C2 and *C. limosum* C3 toxins to have become a VIP1 interaction component[14]. Significant sequence similarity between VIP2 and other actin-ADP-ribosylating binary toxins (with >32% sequence identity) suggests that both the N- and C-domains will have similar folds and likely similar domain packing and domain specialization (Fig. 2).

NAD binding and catalytic mechanism

VIP2 catalytic rate enhancement of actin-ADP ribosylation and concomitant NAD-glycohydrolase activity is an inherently paradox originally pointed out by Cordes and co-workers[15]. The predicted lifetime for a glucopyranosyl oxocarbenium in solution is $<10^{-12}$ s and is believed to be of similar stability as the glycofuranosyl oxocarbenium[16] implicated in cleavage of the glycosylic bond of NAD[17–21]. These intermediate lifetimes are problematically near the bond vibration rate of 10^{-13} s (refs 22,23). Transition state stabilization, either by enzyme or by nucleophile, is likely to be required to allow the reaction to proceed efficiently. For both the ADP ribosylation of Arg 177 and hydrolysis of NAD, no strongly polarizable nucleophile is available that is analogous to the cysteine thiolates observed in the ADP ribosylation of the biological target of pertussis toxin[19,21]. Thus, VIP2 must catalyze breakage of the C1'-N glycosylic bond and formation of an oxocarbenium ion-like transition state in the absence of strong bond formation to the nucleophile as observed in hydrolysis of NAD in other ADP-ribosylases[16–18,20] and energetically distinguish between the positively charged NAD and the positively charged oxocarbenium transition state.

To understand the active site key features to NAD binding and catalysis, a VIP2–NAD complex was kinetically trapped from the slower NAD-glycohydrolase activity by cocrystallizing VIP2 with NAD followed by rapid freezing in liquid nitrogen temperature within 8 h. The rapid growth of diffraction quality VIP2–NAD complex crystals allowed for a protocol for trapping the complex structures that differed from the cryotrapping experiments used in diphtheria toxin-NAD complex[24], in which excess NAD was added to pregrown crystals. The structural details of these reactant complex crystals suggests that rate enhancement is driven more by ground state destabilization than by transition state stabilization (Fig. 3*a–c*).

The VIP2 structures suggest that binding of the nicotinamide ring is a major contributor to ground state destabilization of the substrate. The positively charged ring is desolvated and bound at the edge of and displaced from a hydrophobic

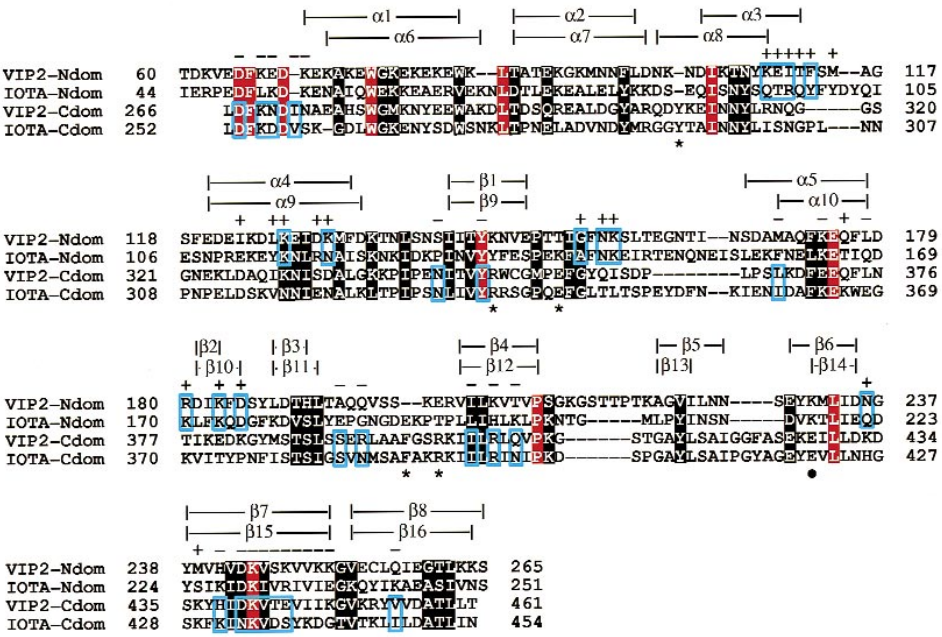

Fig. 2 A structure-based sequence alignment of the *Bacillus cereus* VIP2-N-domain (VIP2-Ndom) with the C-domain (VIP2-Cdom) and with both N-terminal (IOTA-Ndom) and C-terminal (IOTA-Cdom) segments of the *C. perfringens* iota toxin (GeneBank accession number 2127361). The locations of secondary structure elements in the N- and C-domain of VIP2 are indicated over the aligned sequences. Identical residues and similar residues (those that are identical in three sequences) are indicated with red and black background, respectively. Residues at the interdomain interface are marked by + for N-domain and by – for C-domain and are boxed if they are identical or chemically similar in each domain. The catalytic residue, Glu 428 in VIP2, is marked by • beneath the sequences. Residues involved in NAD binding are indicated with an asterisk.

pocket composed of Trp 350, Leu 394, Ala 396 and Phe 397 (Fig. 1*d*) with the carboxamide group forming hydrogen bonds to the Trp 350 main chain carbonyl and amide group. Intriguingly, gas phase studies on the stability of nicotinamide nucleosides suggest that solvent is critical for stability[25]. Besides possible charge stabilization, the solvent cage appears to impede the diffusion of the nicotinamide ring upon transient bond cleavage, promoting recombination with the ribose oxocarbenium. Thus, the presence of the nicotinamide at the edge of a deeper hydrophobic pocket may provide a solvent-free pathway for nicotinamide diffusion and sequestration to avoid recombination in VIP2 and in other ADP-ribosylases[17]. Importantly, as proposed for diphtheria toxin[18], the disassociative transition state observed for NAD cleavage should place the nicotinamide moiety more deeply in the pocket than for the observed reactant complex.

Protein and phosphate group interactions should provide transition state stabilization of the oxocarbenium intermediate, which presumably increases the lifetime of the oxocarbenium ion. Glu 428 Oε1 forms a hydrogen bond with the O2' hydroxyl of the nicotinamide ribose, which increases electronic density on the ring and stabilizes the oxocarbenium ion in a manner roughly analogous to the proposed diol anion-assisted disassociative cleavage observed for NAD in solution above pH 12.5 (ref. 26). The conservation of this glutamate is widespread, and its role in hydrogen bonding the 2'-hydroxyl of the nicotinamide sugar has also been observed in crystal structures of *Pseudomonas aeruginosa* exotoxin A complexed with a NAD analog[12]. Although it has been proposed that the conserved glutamic acid deprotonates the 2'-hydroxyl[26], this is not consistent with observed kinetic isotope effects[20]; however, hydrogen bond formation may satisfy the requirement for increased electron density near C1' to stabilize the oxocarbenium without requiring proton transfer in the transition state. Mutagenesis of the equivalent Glu 428 to Gln in both *C. perfringens* iota[27] and *C. botulinum* C2[28] toxins blocks ADP-ribosyltransferase activity. Compounds that eliminate this stabilization by replacing the ribose 2'-hydroxyl with H or F are inactive[16]. Additionally, NAD binding as a compact moiety may also allow the oxocarbenium ion to be stabilized by its phosphate. Although the reactive end of NAD is similar to that in complex with biologically inactive form of diphtheria toxin including an energetically unfavorable eclipsed glycosylic bond[29], the equivalent glutamate in diphtheria toxin does not form a hydrogen bond with the 2'-hydroxyl of NAD[24]. Additionally, the bond orders of the NAD hydrolysis transition state for diphtheria toxin[18] are substantially different from both cholera toxin[17] and pertussis toxin[20], and are more similar to nonenzymatic solvolysis[30], in which the oxocarbenium-like transition state is stabilized by the incoming nucleophile rather than by the enzyme active site.

VIP2 binding to the phosphates and the adenine ring of NAD is likely to be involved in increasing affinity to the substrate and is not obviously involved in enzymatic rate enhancement. Although two phosphates are not in direct contact with protein in the crystal structure of diphtheria toxin with NAD[24], both NAD phosphates bind arginines from the catalytic domain (Arg 349, Arg 400) that are conserved among the actin-ribosylating binary toxins. Mutagenesis of the equivalent Arg 349 to lysine or alanine in both *C. perfringens* iota[27] and *C. botulinum* C2[28] toxins shows drastic decrease in ADP ribosylation and cytotoxic activities. The adenine fits into a polar pocket composed of the nonconserved Arg 315, Asp 318, Lys 379, Asp 381 and the conserved Glu 355 (Fig. 3*b*).

A conserved sequence (residues 386–388), called the 'STS motif' lies at the end of C-domain β11 and stabilizes the NAD-binding pocket by connecting two perpendicular β-sheets. Besides this structural role of the STS motif, the Ser 386 side chain forms a hydrogen bond to Glu 428 Oε2 to position Glu 428 near the ribose ring 2'-hydroxyl group. Importantly, mutation of the equivalent Ser 386 to alanine in *C. botulinum* C2 toxin eliminates ADP-ribosyltransferase activity[28].

Intriguingly, mutagenesis of the equivalent Glu 426 to Gln in *C. botulinum* C2 toxin separates ADP-ribosyltransferase activity from NAD-glycohydrolase activity[28]. Consistent with this result, the Glu 426 is outside the NAD-binding cleft, on the solvent-exposed loop connecting strand β13 and β14, where it may act in deprotonation of actin Arg 177 to increase

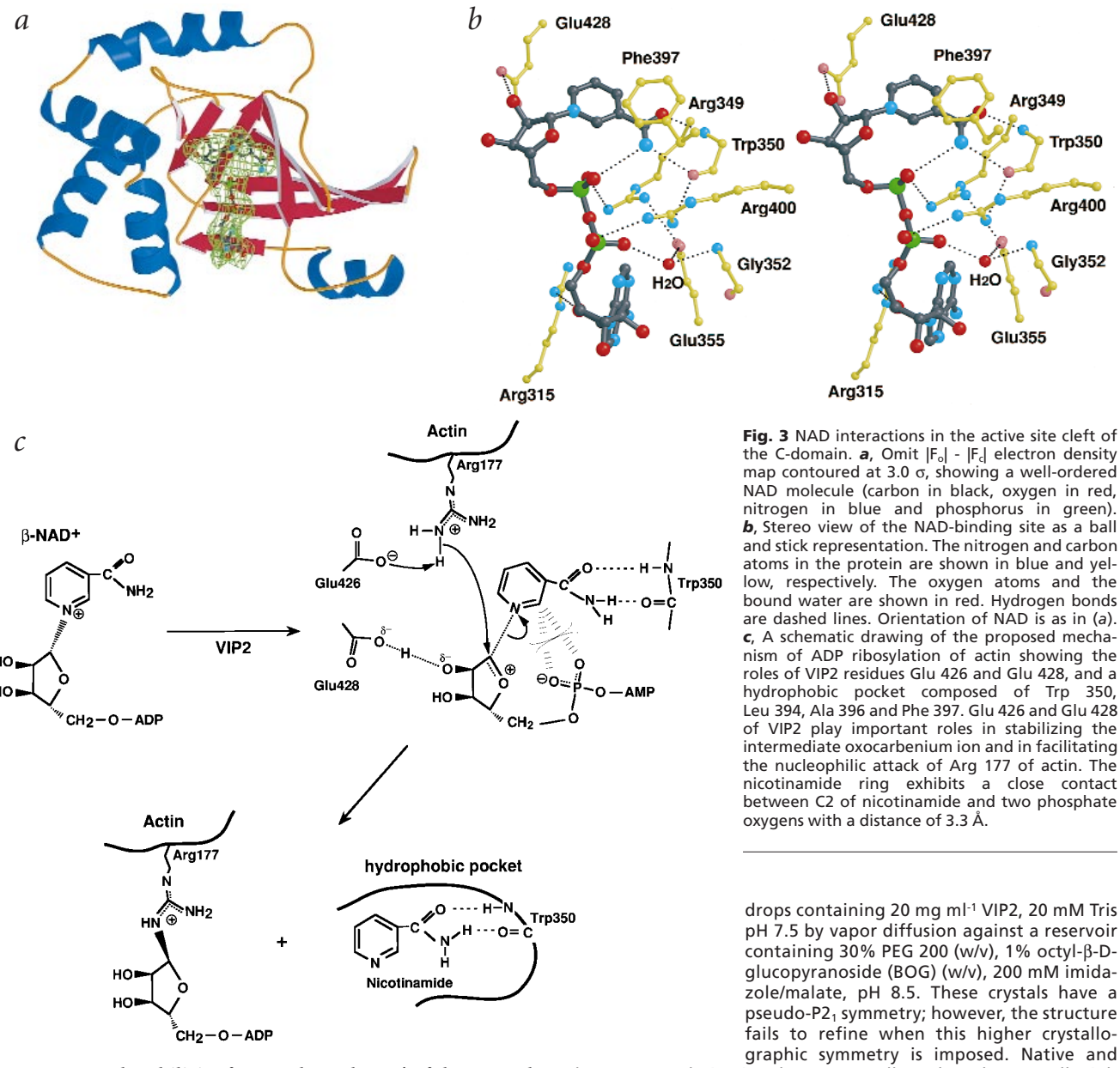

Fig. 3 NAD interactions in the active site cleft of the C-domain. ***a***, Omit $|F_o| - |F_c|$ electron density map contoured at 3.0 σ, showing a well-ordered NAD molecule (carbon in black, oxygen in red, nitrogen in blue and phosphorus in green). ***b***, Stereo view of the NAD-binding site as a ball and stick representation. The nitrogen and carbon atoms in the protein are shown in blue and yellow, respectively. The oxygen atoms and the bound water are shown in red. Hydrogen bonds are dashed lines. Orientation of NAD is as in (*a*). ***c***, A schematic drawing of the proposed mechanism of ADP ribosylation of actin showing the roles of VIP2 residues Glu 426 and Glu 428, and a hydrophobic pocket composed of Trp 350, Leu 394, Ala 396 and Phe 397. Glu 426 and Glu 428 of VIP2 play important roles in stabilizing the intermediate oxocarbenium ion and in facilitating the nucleophilic attack of Arg 177 of actin. The nicotinamide ring exhibits a close contact between C2 of nicotinamide and two phosphate oxygens with a distance of 3.3 Å.

Arg 177 nucleophilicity for attack on the C1' of the oxocarbenium ion upon actin binding to VIP2–NAD complex (Fig. 3*c*).

Taken together, the crystal structures of VIP2 and its NAD complex provide a structural basis for understanding binary toxins and explain the properties of available mutants from these toxins. In establishing structures for the class of binary toxins and the crystallized functional complex with NAD, these structures define chemical, structural and mechanical changes associated with ADP-ribosylating activity. Interestingly, these results suggest how the enzyme may be able to destabilize substrate to promote catalysis that merits further experimental and theoretical analysis.

Methods

VIP2 structure. The VIP2 crystals of space group of P1 (cell dimensions of a = 53.90 Å, b = 78.74 Å, c = 105.95 Å and α = 108.65°, β = 89.96°, γ = 90.02°, four molecules per asymmetric unit, solvent content = 44%) were grown overnight at 20 °C from drops containing 20 mg ml^{-1} VIP2, 20 mM Tris pH 7.5 by vapor diffusion against a reservoir containing 30% PEG 200 (w/v), 1% octyl-β-D-glucopyranoside (BOG) (w/v), 200 mM imidazole/malate, pH 8.5. These crystals have a pseudo-$P2_1$ symmetry; however, the structure fails to refine when this higher crystallographic symmetry is imposed. Native and heavy atom derivative data were collected at the Cornell High Energy Synchrotron Source (CHESS) on beamline F-1 and Advanced Light Source (ALS) on beamline 5.0.1. All data were processed with DENZO and SCALEPACK[31]. Subsequent calculations were carried out with the CCP4 program suite[32]. Initial EMTS mercury sites were determined from an isomorphous difference Patterson map. Positions of other heavy atoms were located by difference Fourier analysis and refined with MLPHARE[32]. The overall figure of merit from 20.0 Å to 2.3 Å resolution is 0.52. After density modification with solvent flattening, histogram matching and NCS averaging in the program DM[32], the atomic model for residues 60–461 was built with the program O[33]. Maximum-likelihood refinement, bulk solvent correction and individual temperature (B) factors were used for the refinement, as implemented in CNS[34]. The Ramachandran plot analysis with PROCHECK[35] showed that 99.4% of the residues in the current model are in the most favorable and additionally allowed regions. The average refined B factor of the VIP2 model is 24.8 Å^2. The N-terminal 56-residue signal peptide is cleaved as the preprotein traverses the cytoplasmic membrane[4] and the three N-terminal residues (residues 57–59) and the C-terminal residue (residue 462) of the mature 46 kDa protein were not observed.

Table 1 Diffraction data and refinement statistics for VIP2 and VIP2–NAD complex

Data set[1]	VIP2	VIP2-NAD	EMTS	PCMB	$Hg(CN)_2$	K_2OsCl_6	K_2IrCl_6	Me_3PbAc
Resolution (Å)[2]	1.5 (1.55–1.50)	2.7 (2.80–2.70)	3.1 (3.21–3.10)	2.3 (2.38–2.30)	1.8 (1.86–1.80)	3.1 (3.21–3.10)	2.3 (2.38–2.30)	2.3 (2.38–2.30)
Observations								
Overall	468,627	118,889	62,188	101,243	238,473	32,770	153,105	118,573
Unique	215,237	15,370	27,768	60,496	138,138	20,827	68,688	58,863
Completeness (%)	83.4 (69.2)	97.7 (99.9)	96.7 (94.5)	85.9 (76.9)	92.0 (76.3)	71.0 (69.1)	96.1 (93.5)	81.4 (76.9)
R_{merge} (%)[3]	4.6 (27.0)	9.8 (30.9)	13.1 (30.5)	7.4 (25.9)	5.3 (10.5)	11.6 (25.8)	7.8 (20.1)	8.7 (23.7)
R_{iso} (%)[4]	–	–	24.4	18.8	23.0	16.5	18.0	28.0
Phasing power[5]	–	–	0.81	1.37	1.29	0.44	0.99	1.08
Sites	–	–	8	4	8	4	4	8

Refined structure	VIP2	VIP2-NAD
Resolution (Å)	20.0–1.5	20.0–2.7
No. of reflections	215,166	15,323
R factor (%)		
R_{cryst}[6]	23.5	20.7
R_{free}[7]	26.9	26.5
No. of non-H atoms		
Protein	12,828	3,200
NAD	–	44
Water	1,501	145
R.m.s.d		
Bonds (Å)	0.006	0.007
Angles (°)	1.30	1.45

[1]The derivative crystals are as follows: EMTS, sodium ethylmercurithiosalicylate; PCMB, *p*-chloromercuribenzoate; $(Me)_3PbAc$, trimethyllead acetate.
[2]Highest resolution of the data set followed in brackets by the range of resolution in the highest resolution bin for compiling statistics.
[3]$R_{merge} = \Sigma_h\Sigma_i |I_{hi} - \langle I_{hi}\rangle| / \Sigma_h\Sigma_i |I_{hi}|$, where h specifies unique reflection indices, i indicates symmetry equivalent observations of h, and $\langle I_{hi}\rangle$ is the mean value.
[4]$R_{iso} = \Sigma_h ||F_{ph}| - |F_p|| / \Sigma_h|F_p|$, where $|F_{ph}| - |F_p|$ are the measured structure factor amplitudes of the derivative and native structures.
[5]The phasing power is the ratio of the structure factor amplitude for the added atoms in a derivative to the estimated error in the phasing model (closure error).
[6]$R_{cryst} = \Sigma||F_o| - |F_c|| / \Sigma|F_o|$ for all reflections (no σ cutoff), where F_o and F_c are the observed and calculated structure factors, respectively.
[7]R_{free} was calculated against 10% of the reflections removed at random for both VIP2 and VIP2–NAD complex data.

VIP2–NAD complex structure. The VIP2–NAD complex crystals of space group $P2_12_12_1$ (cell dimensions a = 53.67 Å, b = 70.56 Å, c = 142.61 Å, one molecule per asymmetric unit, solvent content = 45%) were grown for 8 h at 20 °C by vapor diffusion method. Crystallization solution contained 10% PEG 200 (w/v) and 20% 2-methyl 2,4-pentanediol (v/v), 20 mM β-NAD^+, 1% BOG (w/v) and 100 mM bis-Tris pH 8.0. The data set for crystals of VIP2-NAD complex was collected in-house on a MAR image plate detector mounted on a Rigaku X-ray source at -170 °C. An initial molecular replacement solution (correlation coefficient = 75.0% and R factor = 27.9% for 8–3 Å resolution data) was found by AMoRe[36] by using the native VIP2 model as a probe. The VIP2–NAD complex structure was refined by using the program CNS[34].

Coordinates. Coordinates for the VIP2 wild type structure and the NAD complex have been deposited with the Protein Data Bank under the accession codes 1QS1 and 1QS2, respectively.

Acknowledgments
We thank D.S. Daniels, J.L. Pellequer, T.P. Lo and C.M. Bruns for insightful discussions, and facilities at ALS and CHESS. Work on VIP2 was supported in part by the Skaggs Institute for Research and by Novartis Agribusiness Biotechnology Research Inc. C.D.P. was supported by a Howard Hughes Predoctoral Fellowship and J.A.T. by the NSF.

Correspondence should be addressed to J.A.T. *email: jat@scripps.edu*

Received 19 May,1999; accepted 6 July, 1999.

1. Warren, G.W. In *Advances in insect control: the role of transgenic plants.* (eds Carozzi, N.B. & Koziel, M.G.) 109–121 (Gunpowder Square, London, United Kingdom; 1997).
2. Nishimatsu, T. & Jackson, J. J. *J. Econ. Entomol.* **91**, 410–418 (1998).
3. Madshus, I.H. & Stenmark, H. *Curr. Top. Microbiol. Immunol.* **175**, 1–26 (1992).
4. Warren, G.W. *et al. Novel pesticidal proteins and strains.* World Intellectual Property Organization. Patent WO 96/10083 (1996).
5. Carlier, M.-F. *Int. Rev. Cytol.* **115**, 139–170 (1989).
6. Aktories, K. *et al. Nature* **322**, 390–392 (1986).
7. Stiles, B.G. & Wilkens, T.D. *Infect. Immunol.* **54**, 683–688 (1986).
8. Simpson, L.L., Stiles, B.G., Zepeda, H. & Wilkins, T.D. *Infect. Immunol.* **57**, 255–261 (1989).
9. Popoff, M.R., Rubin, E.J., Gill, D.M. & Boquet, P. *Infect. Immunol.* **56**, 2299–2306 (1988).
10. Sixma, T.K. *et al. Nature* **351**, 371–377 (1991).
11. Bell, C.E. & Eisenberg, D. *Biochemistry* **36**, 481–488 (1997).
12. Li, M., Dyda, F., Benhar, I., Pastan, I. & Davies, D.R. *Proc. Natl. Acad. Sci. USA* **93**, 6902–6906 (1996).
13. Aktories, K., Weller, U. & Chhatwal, G.S. *FEBS Lett.* **212**, 109–113 (1987).
14. Barth, H., Hofmann, F., Olenik, C., Just, I. & Aktories, K. *Infect. Immunol.* **66**, 1364–1369 (1998).
15. Bull, H.G., Ferraz, J.P., Cordes, E.H., Ribbi, A. & Apitz–Castro, R. *J. Biol. Chem.* **253**, 5186–5192 (1978).
16. Oppenheimer, N.J. *Mol. Cell. Biochem.* **138**, 245–251 (1994).
17. Rising, K.A. & Schramm, V.L. *J. Am. Chem. Soc.* **119**, 27–37 (1997).
18. Berti, P.J., Blanke, S.R. & Schramm, V.L. *J. Am. Chem. Soc.* **119**, 12079–12088 (1997).
19. Scheuring, J. & Schramm, V.L. *Biochemistry* **36**, 8215–8223 (1997).
20. Scheuring, J. & Schramm, V.L. *Biochemistry* **36**, 4526–4534 (1997).
21. Scheuring, J., Berti, P.J. & Schramm V.L. *Biochemistry* **37**, 2748–2758 (1998).
22. Banait, N.S. & Jencks, W.P. *J. Am. Chem. Soc.* **113**, 7958–7963 (1991).
23. Cherian, X.M., Van Arman, S.A. & Czarnik, A.W. *J. Am. Chem. Soc.* **112**, 4490–4498 (1990).
24. Bell, C.E. & Eisenberg, D. *Biochemistry* **35**, 1137–1149 (1996).
25. Buckley, N., Handlon, A.L., Maltby, D., Burlingame, A.L. & Oppenheimer, N.J. *J. Org. Chem.* **59**, 3609–3615 (1994).
26. Johnson, R.W., Marschner, T.M. & Oppenheimer, N.J. *J. Am. Chem. Soc.* **110**, 2257–2263 (1988).
27. Perelle, S., Domenighini, M. & Popoff, M.R. *FEBS Lett.* **395**, 191–194 (1996).
28. Barth, H., Preiss, J.C., Hofmann, F. & Aktories, K. *J. Biol. Chem.* **273**, 29506–29511 (1998).
29. Bell, C.E., Yeates, T.O. & Eisenberg, D. *Protein Sci.* **6**, 2084–2096 (1997).
30. Berti, P.J. & Schramm, V.L. *J. Am. Chem. Soc.* **119**, 12069–12078 (1997).
31. Otwinowski, Z. & Minor, W. *Methods Enzymol.* **276**, 307–326 (1997).
32. Collaborative Computational Project, Number 4. *Acta Crystallogr. D* **50**, 760–763 (1994).
33. Jones, T.A., Zhou, J.-Y., Cowan, S.W. & Kjeldgaard, M. *Acta Crystallogr. A* **47**, 110–119 (1991).
34. Brünger, A.T. *et al. Acta Crystallogr. D* **54**, 905–921 (1998).
35. Laskowski, R.A., MacArthur, M.W., Moss, D.S. & Thornton, J.M. *J. Appl. Crystallogr.* **26**, 283–291 (1993).
36. Navaza, J. *Acta Crystallogr. A* **50**, 157–163 (1994).
37. Kraulis, P.J. *J. Appl. Crystallogr.* **24**, 946–950 (1991).